Realizing high thermoelectric performance in highly (0l0)-textured flexible Cu2Se thin film for wearable energy harvesting

Z.-H. Zheng, D.-L. Zhang, B. Jabar, T.-B. Chen, M. Nisar, F. Li, S. Chen, G.-X. Liang, Xianghua Zhang, P. Fan, et al.

Zhuang-Hao Zheng: Conceptualization; Methodology;Formal analysis; Investigation; Resources; Data Curation; Writing - Original Draft; Project administration; Funding acquisition. **Dong-Liang Zhang:** Methodology; Formal analysis. **Bushra Jabar:** Methodology; Formal analysis. **Tian-Bao Chen:**Data Curation. **Mohammad Nisar :** Formal analysis. **Yun-Fei Chen:** Formal analysis. **Fu Li:** Formal analysis; Resources. **Shuo Chen：** Formal analysis; **Guang-Xing Liang:** Formal analysis; Resources. **Xiang-Hua Zhang**:Investigation; Resources. **Ping Fan：** Supervision; Project administration. **Yue-Xing Chen:** Conceptualization; Methodology; Validation; Formal analysis; Resources; Data Curation; Writing - Review & Editing;

Graphical Abstract

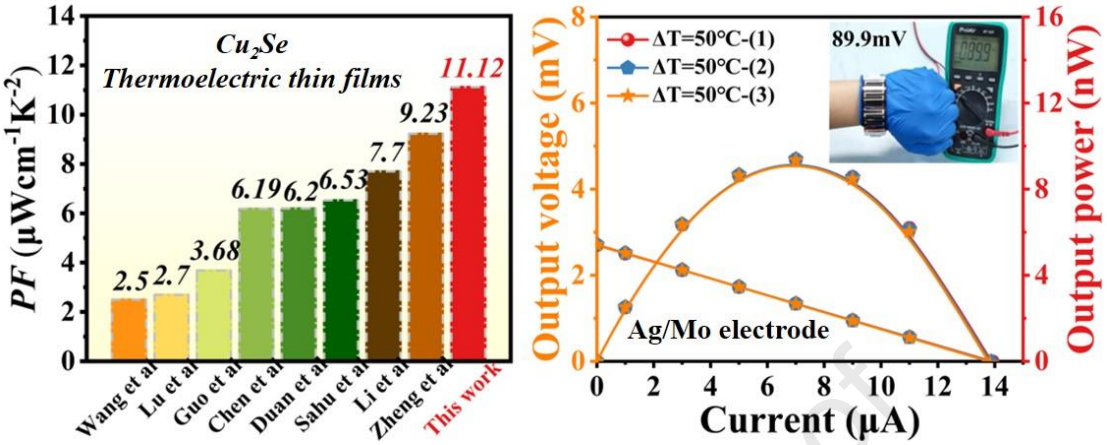

Realizing high thermoelectric performance in highly (0*l*0)-textured flexible Cu_2Se thin film for wearable energy harvesting

Zhuang-Hao Zheng[a], Dong-Liang Zhang[a], Bushra Jabar[a], Tian-Bao Chen[a,b], Mohammad Nisar[a], Yun-Fei Chen[c], Fu Li[a], Shuo Chen[a], Guang-Xing Liang[a], Xiang-Hua Zhang[b], Ping Fan[a], Yue-Xing Chen[a]*

a Shenzhen Key Laboratory of Advanced Thin Films and Applications, Key Laboratory of Optoelectronic Devices and Systems of Ministry of Education and Guangdong Province, College of Physics and Optoelectronic Engineering, Shenzhen University, Shenzhen 518060, P. R. China

b Univ Rennes, CNRS, ISCR (Institut des Sciences Chimiques de Rennes) UMR6226, Rennes, F-35000, France

c Hangzhou Innovation Institute, Beihang University, Hangzhou, 310052, P. R. China

* Corresponding author, E-mail: chenyx@szu.edu.cn

Abstract

Searching for eco-friendly and earth-abundant materials to supersede traditional high-cost bismuth telluride for fabricating wearable devices is of great significance in thermoelectrics. In this work, promising flexible Cu_2Se based thin films with high thermoelectric performance is successfully fabricated via a facile co-sputtering method. Experimental results indicate that excess Cu in Cu_2Se films leads to the decrease of carrier concentration by suppressing the formation of Cu vacancies and donating electrons, benefiting to achieve high Seebeck coefficient. Moreover, Cu-excess Cu_2Se films have highly (0*l*0) preferred orientation and contribute to the extra high carrier mobility, maintaining the decent electrical conductivity in the whole measurement temperature range. Combined with the

low thermal conductivity, a maximum *ZT* of 0.42 is obtained at 275 °C from the Cu-excess Cu_2Se due to the simultaneous optimization both of electrical and heat transport. Subsequently, a flexible thermoelectric device assembled with high performance Cu_2Se films exhibits a maximum power density of 4.28 Wm^{-2} at a temperature difference of 50 °C, which thermal stability is greatly improved after introducing a molybdenum buffer layer into electrode layer. Therefore, this work demonstrates that rational microstructure manipulations and connection technology improvement can achieve high performance in the flexible thermoelectric device, which possess potential in wearable applications.

Keywords Thermoelectric; Cu_2Se; Flexible thin film; Figure of merit

1. Introduction

Owing to portable use experience, more and more wearable microelectronic devices have gradually entered the public view [1]. Accordingly, the demand for finding a sustainable self-powered generator for wearable devices instead of using traditionally bulky charging power equipment is urgent [2]. A flexible thermoelectric (TE) thin film device, which can directly converse heat into electricity, is one of the highly expected candidates to realize self-powered by using the temperature difference between the human body and external environment [3]. The efficiency of thermoelectric device is mainly depended on figure of merit *ZT* ($ZT=S^2\sigma T/\kappa$, where S, σ, κ and T is Seebeck coefficient, electrical conductivity, thermal conductivity, and absolute temperature, respectively.) of the thermoelectric materials. Distinctly, thin films need a high power factor ($PF=S^2\sigma$) and low thermal conductivity to achieve high thermoelectric conversion efficiency in the device. To data, $(Bi, Sb)_2Te_3$ based materials are the preferred choice for fabricating thin film device due to their high thermoelectric performance at near room temperature [4, 5]. However, compared with equivalent bulks in most reports, the *ZT* values of $(Bi, Sb)_2Te_3$ thin film are low [6, 7]. On the other hand, even if high power factor can be produced, large-scale application of $(Bi,Sb)_2Te_3$ film will still be limited due to toxicity and high cost of its component; hence, the challenge for thin-film TE device is to find eco-friendly, low-cost, and high *ZT* value thin films.

In recent decades, eco-friendly bulk thermoelectric materials have made significant progresses as the *ZT* values had been promoted over 1.5 in some material systems [8-14]. For example, *ZT* values reached 2.0 were reported for both PbTe bulk and layered polycrystalline SnSe [9-10]. The GeTe compound via the vacancy suppression and band structure engineering strategy with Bi doing led to a high *ZT* of 2.0 [11]. However, most of the mentioned materials exhibit the maximum *ZT* over 600 K,

but have poor TE performance at near room temperature range. Non-toxic and earth-abundant Cu_2Se is one of the most studied TE materials which maximum *ZT* achieved 1.8 for pure Cu_2Se [12-13] and the *ZT* can be further increased to 2.62 by Al doping [14]. The high TE performance is attributed to its special "liquid-like" behavior of the anti-fluorite-structured *β*-phase. More specially, the experimental result also indicates Cu_2Se with monoclinic structured α-phase below 400 K has relatively high *ZT* value over 0.6 [15] and predicts over 1.1 [16], which is comparable with that of the traditional $(Bi, Sb)_2Te_3$. Therefore, Cu_2Se provides an exciting commercial opportunity as a potential substitute for fabricating high-efficiency and low-cost flexible thin-film devices. Many works focused on obtaining high-performance Cu_2Se thin films have been reported in recent years [17-21]. To data, carrier engineering is the most effective method to improve the TE performance of Cu_2Se thin films. For instance, Jin's team proposed that carrier localization increased Seebeck coefficient by fullerenes doping, and the synergistic enhancement of phonon scattering led to reduction of thermal conductivity, resulting in a 20-30% improvement in *ZT* at 773K [22]. Coincidentally, Chen's group optimized the phonon and carrier transport performance by alloying cuprous selenide with Cu_2Se based, achieving a 45% increase in power factor at 300K and an average 24% increase ZT values between 300K and 390K [23]. Carriers transport properties may be further optimized with controllable composition of Cu_2Se film, as Cu atoms play an important role in the matrix [24].

In our previous work, a similar strategy was employed which resulted in high power factor of 5.3 $\mu Wcm^{-1}K^{-2}$ at 300 K in Cu_2Se thin films deposited at solid substrate [24]. The carrier transport of films was significantly improved with enhancement of growth preferred orientation via heat treatment. Based on the density calculation and the experimental analysis, we confirmed the Cu_2Se thin film with (0*l*0) preferred orientation has higher energy barrier, which will inhibit the bipolar effect and block the

minority carriers, benefiting in achieving high Seebeck coefficient and contributing in the enhancement of power factor. However, Cu_2Se thin film prepared at flexible substrate by using the same method has poor electrical transport properties compared with the films deposited on solid substrate due to the poor crystallinity [25]. Therefore, in this work, a facile co-sputtering method was employed to fabricate Cu_2Se films on flexible substrate by controlling the accurately composition between Cu and Se, and an annealing process was further used to improve the crystallinity of the films. Microstructure analysis indicates that thin films have single Cu_2Se α-phase with highly (0*l*0) preferred growth orientation when the Cu/Se composition ratio is over 2.17. These films have high Seebeck coefficient and moderate electrical conductivity, resulting in high power factor. Meanwhile, low thermal conductivity is also found in the Cu-excess thin films due to the introduced point defects in lattice, which can enhance the phonons scattering and lead to low lattice thermal conductivity. Consequently, a maximum *ZT* of 0.42 is obtained in the Cu_2Se thin films at 275 °C, which is higher than most of flexible Cu_2Se based thin films and can even be comparable to the values of bulks at the same measured temperature. Subsequently, traditional silver, molybdenum, aluminium and copper metals are studied as the connecting electrodes of TE Cu_2Se legs, and the results show that Ag has the lowest contact resistance. By further introducing a nanometer thickness of Mo buffer layer to prevent the diffusion of Ag, the thermal stability of the as-fabricated device is greatly improved.

2. Experimental details

A series Cu_2Se thin films with different Cu to Se atomic ratios were prepared using the co-sputtered Cu target (99.9%) and the Cu_2Se alloy target (Cu_2Se, ~99.95%). Flexible polyimide (PI, through rate of 70%) with the thickness of 0.125 mm was used as substrate, and cleaned through detergent, ultrapure water, ethanol, and then through the compression air jet equipment and drying box

for drying treatment. The target powers of Cu_2Se target and Cu target were selected to 55 W and 15 W, respectively. The background pressure was 8×10^{-4} Pa, and working pressure was adjusted to 0.5 Pa by setting the argon gas of 40 sccm. The deposition time of Cu_2Se is 30 min. The samples were annealed in a glove-box heating system in a nitrogen atmosphere at 300 ℃ for 30 min. The thickness of the thin films and composition measured by scanning electron microscope (SEM) and energy dispersive X-ray spectroscopy system (EDS). The thickness of the film was measured using a profilometer (Dektak XT, Bruker). In this work, the atomic ratios of Cu/Se of films are increase gradually with increasing the operating time from 0 min to 11 min (0, 3, 5, 7, 9 and 11 min, respectively) of Cu target during the co-sputtering process. The corresponding samples are named as Cu-0min, Cu-3mins, Cu-5mins, Cu-7mins, Cu-9mins and Cu-11mins, respectively. The corresponding atomic ratios of Cu/Se of films are 1.99, 2.05, 2.17, 2.20, 2.26 and 2.31, respectively. The EDS results are listed in Table S1 (supporting information).

The crystal structure of the film was analyzed by X-ray diffractometer (XRD, Ultima-iv) and the test Angle ranged from 10°to 60°with the scan speed is 2°/min with the CuKα radiation. Preferred orientation information of Cu_2Se thin films was characterized by four-circle X-ray diffractometer (X'PERT, Philips) using pole figure scans. The surface morphology was measured by scanning electron microscope (SEM,Supra55), and depth microstructure was also measured by transmission electron microscopy (TEM, JEM3200FS). The chemical valence states of copper and selenium were characterized by X-ray photoelectron spectroscopy (XPS, Escalab 250Xi) using a monochrome Al-Ka X-ray source. Plasma etching was performed for 30 seconds to remove surface impurities. The electronic band structure and density of states (DOS) for Cu_2Se and Cu-excess Cu_2Se are performed by first-principles plane-wave pseudopotential formalism as implemented in the VASP package, the

calculation detail can be found in Supporting Information.The thickness was measured by a step meter and scanning electron microscope. Carrier concentration was provided by the Hall tester (HL5500PC, Nanometrics) under a reversible magnetic field (0.5 T) by the van der Pauw method. Electrical conductivity and Seebeck coefficients as a function of temperature were provided by the Seebeck conductivity coefficient measurement system (SBA458, Netzsch). Thermal conductivity was measured using the Van-der-Pauw test [26]. The method strictly requires the film to be covered on the chip contact, and the transverse thermal conductivity is measured after the probe touches the contact. The film preparation can be achieved using a pull-0ff foil deposition mask, which is suitable for most film-making processes. The measurement was performed from room temperature to 275 ℃. Keithley 2400 was used to measure IV data of thin film devices and plot curves. The combined uncertainty for the experimental determination of *ZT* is about 15% and is caused by the three respective measurement parameters including σ, S and κ.

3. Results and discussion

To detect structural changes and understand the variation in lattice of Cu_2Se with the change of stoichiometric ratio, we naturally carried out X-ray diffraction analysis. Fig. 1(a) shows XRD patterns of Cu_2Se based films with different stoichiometric ratios at fixed heat treatment temperature. The films presents high temperature phase (β-Cu_2Se, F-43m) for $Cu_{1.99}Se$ and $Cu_{2.05}Se$ samples, which gradually convert to low temperature phase (α-Cu_2Se, Fm-3m) as the increase of Cu content. It is worth noting that high temperature phase β-Cu_2Se is stable at room temperature, which may arise due to the existence of low dimensional effect in the thin film, consistent with the results of the previous study [18]. For the films with composition of Cu-7mins, Cu-9mins, and Cu-11min, the XRD patterns are well indexed as α-Cu_2Se phase (PDF#37-1187), and no second phase is observed. Furthermore, the

diffraction peaks show very strong (*0l0*) orientation (*l*=3,6,9), this can be verified by calculated high orientation factors of (0*l*0) (Fig. S1, Supporting Information) and structure refinement results, as shown in Fig. 1(b) and Fig. S2. (Supporting Information) The (0*l*0) preferred orientation characteristic for α-Cu_2Se phase is further investigated via (030) and (060) X-ray pole figure analysis as shown in Fig. 1(c) and Fig. 1(d). It can be analyzed that there are high peak intensities at 2θ=13.039° (030) and 2θ=26.188° (060). The red and blue areas in the figure indicate high or low polar densities, respectively. Rotating counterclockwise around the vertical X-axis is 0° to 360° in polar coordinates. It can be seen that the test results at all locations indicate that the film has peak intensity gathering points at Phi=35.71°, Phi=95.24° and Phi=152.53°, which exactly represent the three planes of (030), (060) and (090), consisting with the (0*l0*) preferred orientation in XRD patterns (Fig. 1(a)) As shown in Fig.S3 (Supporting Information), there are other peak densities in the film, but their intensity is not as high as the above three positions, so it does not affect the judgment of preference orientation.

XPS measurements were employed on Cu_2Se based thin films (Cu-3mins, Cu-5mins, and Cu-7mins) to study the binding states. As shown in Fig. 1(g), the core-level spectrum exhibits two strongest peaks at ~932.4 eV and ~952.2 eV, respectively, namely, Cu $2p_{3/2}$ and Cu $2p_{1/2}$. It basically matches the spin-orbit phenomenon of Cu (I) [27]. More notably, we do not observe impurity peaks in the spectra, excluding the existence of copper oxidation in this sample. The characterization of Se (-II) in a consistent, cohesive environment [28] is described intuitively in Fig 1 (h). It can be seen that the nearly symmetrical wide peak spans from 54 to 56 eV and this wide peak can be divided into two small peaks, which represent Se $3d_{5/2}$ and Se $3d_{3/2}$, respectively, and refer to two positions ~54.2 and ~54.9 eV. To sum up, the chemical states of elements in thin films prove that only Cu^{1+} and Se^{2-} bonding states can be observed in as-fabricated films. In addition, the weak dependence of peak positions for

Cu and Se elements indicates the stable valence states for all films.

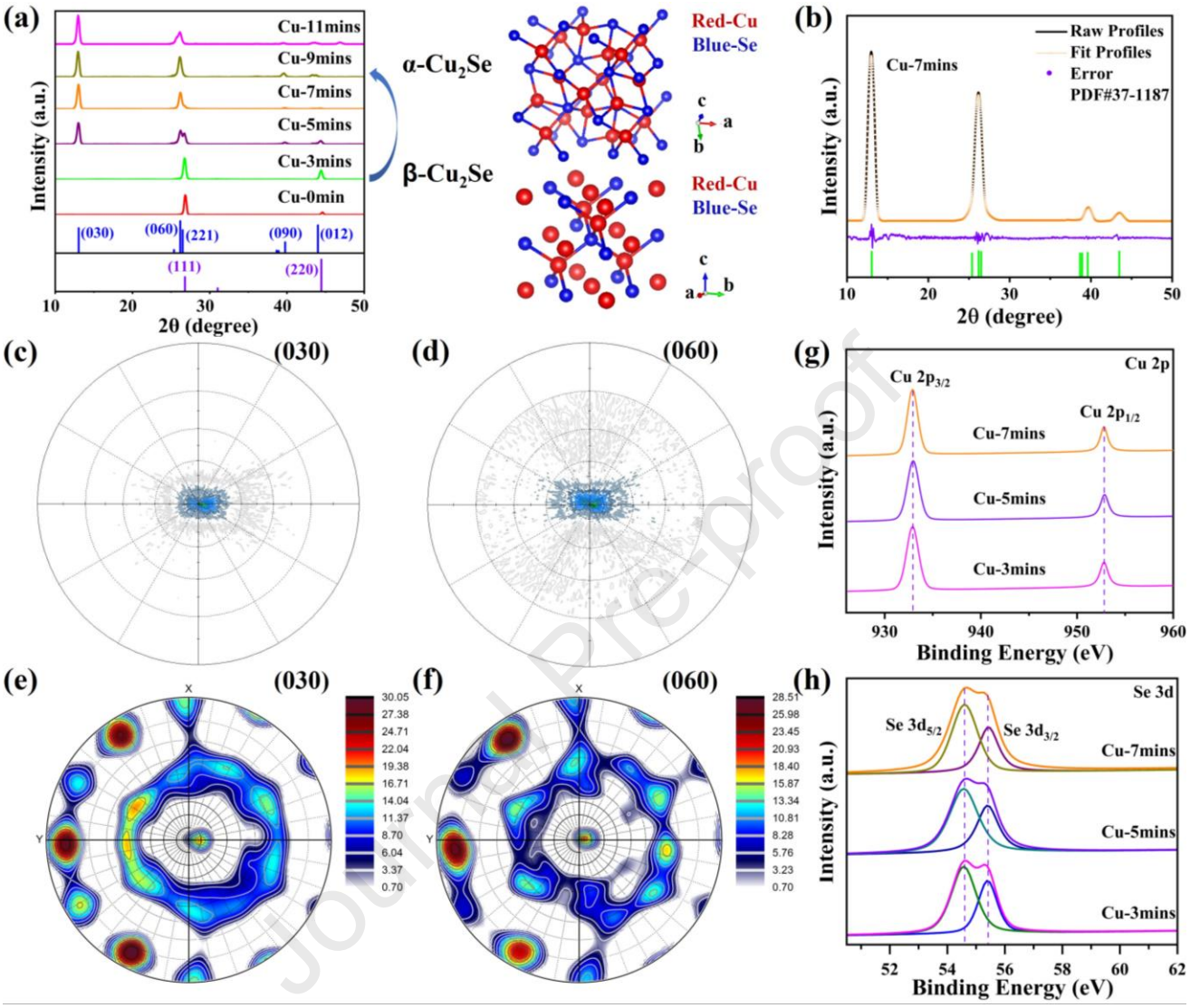

Fig.1. (a) XRD patterns of thin films with different composition ratios at the same heat treatment temperature. (b) XRD refinement of Cu-7mins. (c) 2θ=13.039°and (d) 2θ=26.188° X-ray pole figure XRD pole figures of Cu-7mins.; XRD polar figures of (e) 2θ=13.039° and (f) 2θ=26.188° after ATEX (Analysis Tools for Electron and X-ray diffraction) analysis. (g) XPS spectra of Cu in Cu-3mins, Cu-5mins and Cu-7mins thin films. (h) XPS spectra of Se in Cu-3mins, Cu-5mins and Cu-7mins thin films.

The surface of morphology of the Cu_2Se-based thin film is studied by SEM, as shown in Fig. 2. It can be found that Cu-0min (Fig.2a), Cu-3mins (Fig.2c), as well as Cu-5mins (Fig. S4a) thin films

are growing dense which grains are uniformly distributed with the size ~ 50 nm. The cross-section images reveal the thickness of films is ~400 nm, and the grains are irregular arranged (Fig. 2b). As for the films with higher Cu content, namely Cu-7mins (Fig.2d), Cu-9mins (Fig.2e) and Cu-11mins (Fig. S4b, Supporting Information), most of the grains are growing vertical to the surfaces, which can be further confirmed via the cross-section images (Fig. 2e). The regular growth of the grains has consisted with the high orientation feature as concluded from the XRD patterns and polar diagram analysis (Fig. 1). Fig. 2 (g ~ i) show element mappings of Cu-7mins film, both Cu and Se elements are homogeneously distributed, and no regional aggregation can be observed according to the detectable limit of EDS. Hence, the existence of the extra Cu in the films will be further explored via the micro-structure analysis.

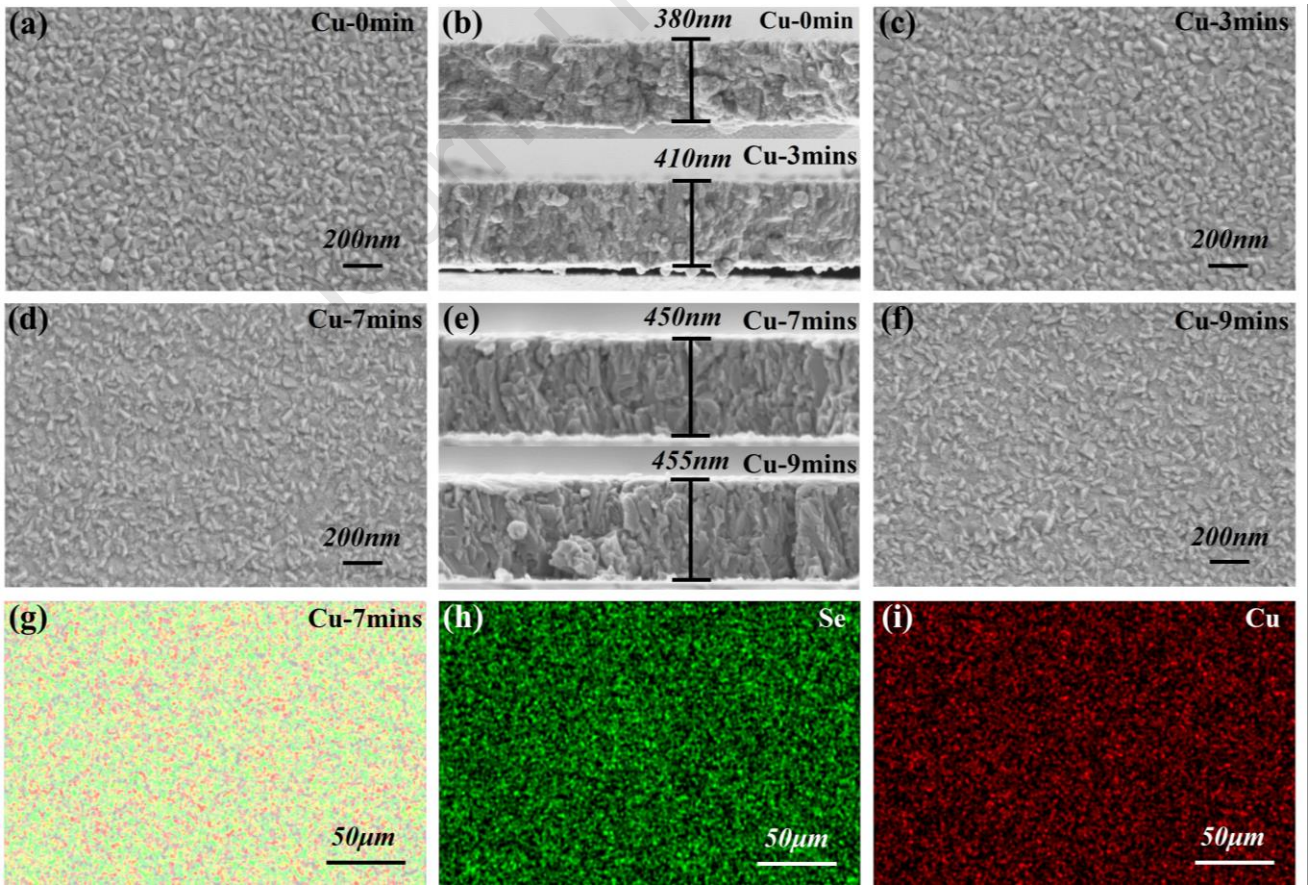

Fig.2. Surface morphologies of the film with different Cu:Se atomic ratios of (a) 1.99:1 (Cu-0min), (c)

2.05:1 (Cu-3mins), (d) 2.20:1 (Cu-7mins), (f) 2.26:1 (Cu-9mins). Cross section morphology of the film for (b) Cu-0min, Cu-3mins , (e) Cu-7mins, and Cu-9mins , respectively. (g)-(h) Elements mapping of the Cu-7mins sample.

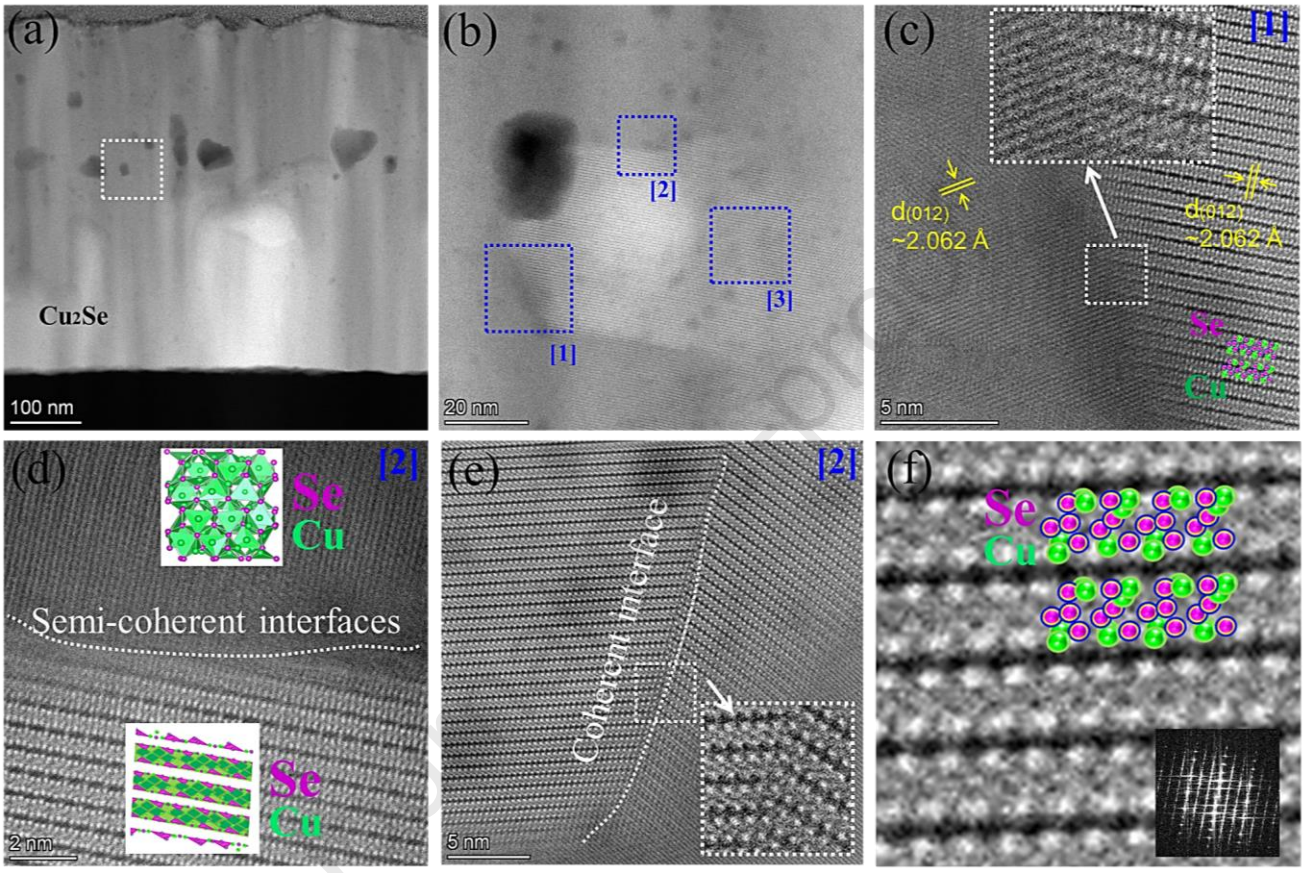

Fig.3. TEM analysis of Cu-7mins thin film; (a) low resolution TEM image, (b) high resolution TEM (HRTEM) image of the selected area in (a) indicates embedded crystalline grains in Cu-7mins thin film, (c) enlarged HRTEM image of selected area [1] in (b), the insets is IFFT images of white-dotted region in (c)), (d) enlarged HRTEM image of selected area [2] in (b), (e) HRTEM image of grain boundary between two crystalline phases clearly indicates coherent phase boundary (selected area [3] in (b)), (f) IFFT images of an area from a crystalline phase.

The extremely high (0*l*0) orientation and the significant improvement of TE performance are

closely related to the excess Cu content for Cu_2Se film; hence, a transmission electron microscopy (TEM) was performed to investigate the microstructure of Cu-7mins film to confirm the existence of excess Cu. Fig.3 (a) shows the low magnification TEM image of Cu-7mins film, in which the high-resolution TEM image marked with white-dotted rectangle is presented in Fig. 3 (b). It can be seen that the grains are embedded in the Cu-7mins film. Fig.3 (c) and Fig.3 (d) show enlarged HRTEM images of selected regions [1] and [2] in Fig (b). The images clearly show the semi-coherent boundary between the highly crystalline phase and the polycrystalline phase. Of course, the crystal plane spacing of (012) in the two figures is approximately 2.062 Å, agreeing with the matrix of Cu_2Se. The HRTEM image (Fig. 3(e)) of grain boundary between two crystalline phases indicates coherent phase boundary. The inverse fast Fourier transform (IFFT) image of an area from a crystalline phase is shown in Fig. 3(f). The IFFT image represents the atomic distribution within α-Cu_2Se atomic framework (Table S1, Supporting Information). Subsequently, the presence of highly crystalline phase and the polycrystalline phase illustrate the atomic models of the two orientations, agreeing with the high (0*l*0) orientation of as fabricated film. In addition, the stress arising from the semi-coherent interfaces in the film (Fig.S5 (Supporting Information)) is conducive to enhancement of phonon scattering and leads to the reduction of the thermal conductivity.

Fig.4(a) and Fig.4(b) show the temperature dependence of electrical conductivity σ and Seebeck coefficient S of Cu_2Se based films with different stoichiometric Cu/Se ratios. It can be seen that both σ and S change regularly with the variation of Cu content, namely, the σ decreases with the increasing of Cu content, while S increases with the increase of Cu content. It is worth noting that the variations in $\sigma(T)$ and $S(T)$ are commonly observed in Cu_2Se based films[19]. To explain the variation of $\sigma$and S, carrier concentration n was measured at room temperature, and the carrier mobility μ was calculated

from the experimental σ and n ($\sigma = ne\mu$, where e is the carrier charge) With increasing Cu content from 1.99 to 2.31 in Cu_2Se films, n is gradually reduced, which is the major factor for the enhancement of S and decrease of σ. That is because the excess Cu will reduce the Cu vacancies and results in the decline of n, consisting with the experimental results of Cu_xSe bulks reported by Shi *et al* [29]. Meanwhile, the mobility of α-Cu_2Se films increased with Cu content (Cu/Se= 2.17~2.31) (Fig.4 (c)), corresponding with the reduction in calculated effect mass m^* (Fig.S6a-6b, Supporting Information), which was calculated using the single parabola band (SPB) model. Obviously, the relative high m^* of films with excess Cu is responsible for the decent S. In addition, due to the phenomenon of high preferred orientation of α-Cu_2Se films, the carrier concentration and mobility of the film are generally higher than that of other reports [20, 30]. The band structures of β-Cu_2Se (Fig.4(d)) and α-Cu_2Se (Fig.4(e)), and corresponding density of states (DOS) (Fig.S7(a)-(b), Supporting information) exhibit narrow band-gap semiconductor characteristic with different orbital energy distribution near the valence band maximum (VBM), which is believed to be caused by the disorder of Cu atoms [31]. It is noteworthy that the slope of density of state (DOS) of α-Cu_2Se near VBM is steeper than that of β-Cu_2Se, consisting with the experimental results of higher Seebeck coefficient of α-Cu_2Se (Fig. 4(b)). Due to the regularly variation in σ and S, a maximum power factor value ~ 8.4 $\mu Wcm^{-1}K^{-2}$ at room temperature for $Cu_{2.20}Se$ thin film, and then increase to 11.12 $\mu Wcm^{-1}K^{-2}$ at 275°C (Fig.4 (f)). As shown in Fig. 4 (g), the high PF is higher than that of other reported films deposited by different methods [17-20, 25, 32-34], including sputtering [17,32], thermal evaporation [18], pulsed laser deposition [19], solution immersion method [20], sputtering combined with thermal evaporation method [25], ion beam sputtering [33], spin coating process [34]. The high PF is also comparable with that of Cu_2Se bulk (PF=12.52 $\mu Wcm^{-1}K^{-2}$) reported by Yu *et al.*. [35] With regard to the thermal

transport properties of the as-fabricated Cu_2Se films, the thermal conductivity κ was measured along the in-plane direction (same measured direction with electrical transport properties), the temperature dependence of κ is plotted in Fig. 4 (h). With increased content of Cu, the κ and κ_l (κ_l is determined from different value of κ and electrical, thermal conductivity κ_e, seen the Fig. S8, Supporting Information) are significantly reduced. This may be attributed to the significantly enhancement of phonons scattering in the films, as the excess Cu atoms can be easily formed as phonon scattering centers and the existence of stress arising from the semi-coherent interfaces helps to block the transport of phonons. Finally, the *ZT*s of the Cu_2Se films were determined (Fig. 4 (i)). A *ZT* value of 0.21 is achieved for Cu-7mins film with Cu:Se atomic ratios of 2.20 : 1 at room temperature, which value gradually increase to 0.42 at 275 ℃.

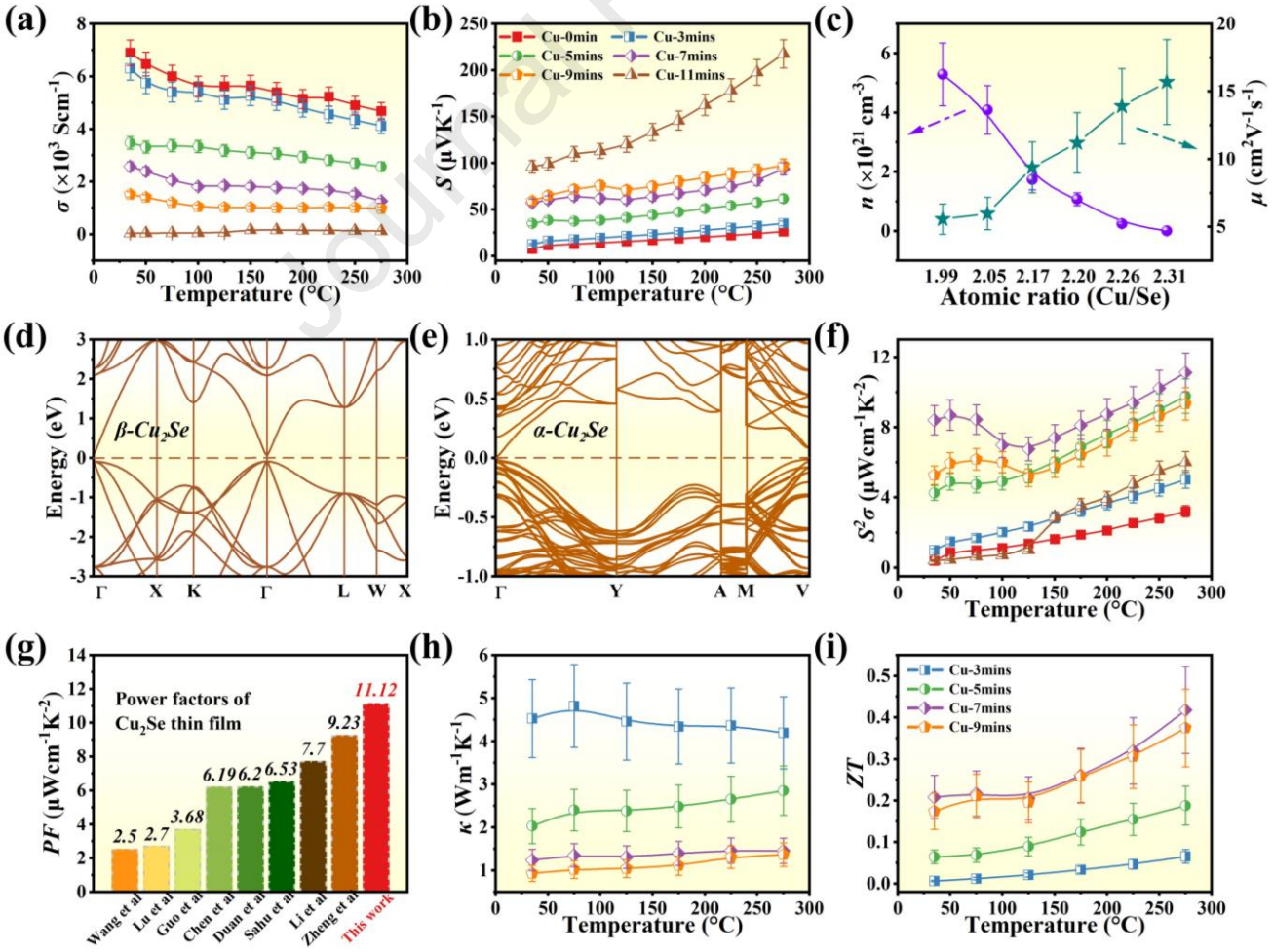

Fig.4. (a) Electrical conductivity of Cu_2Se-based films at different stoichiometric ratios. (b) Seebeck coefficients of Cu_2Se-based films at different stoichiometric ratios. (c) The variation of of mobility and carrier concentration as a function of atomic ratio of Cu/Se. (d)-(e) Electronic band structures of β-Cu_2Se and α-Cu_2Se. (f) Power factor variation of Cu_2Se-based films at different stoichiometric ratios. (g) Comparison of power factors for Cu_2Se based films between this work and other reported films deposited by different methods [17-20, 25, 32-34]. (h) Thermal conductivity of films with different stoichiometric ratios at different temperatures. (i) The ZT values of films with different atomic ratios change at different temperatures.

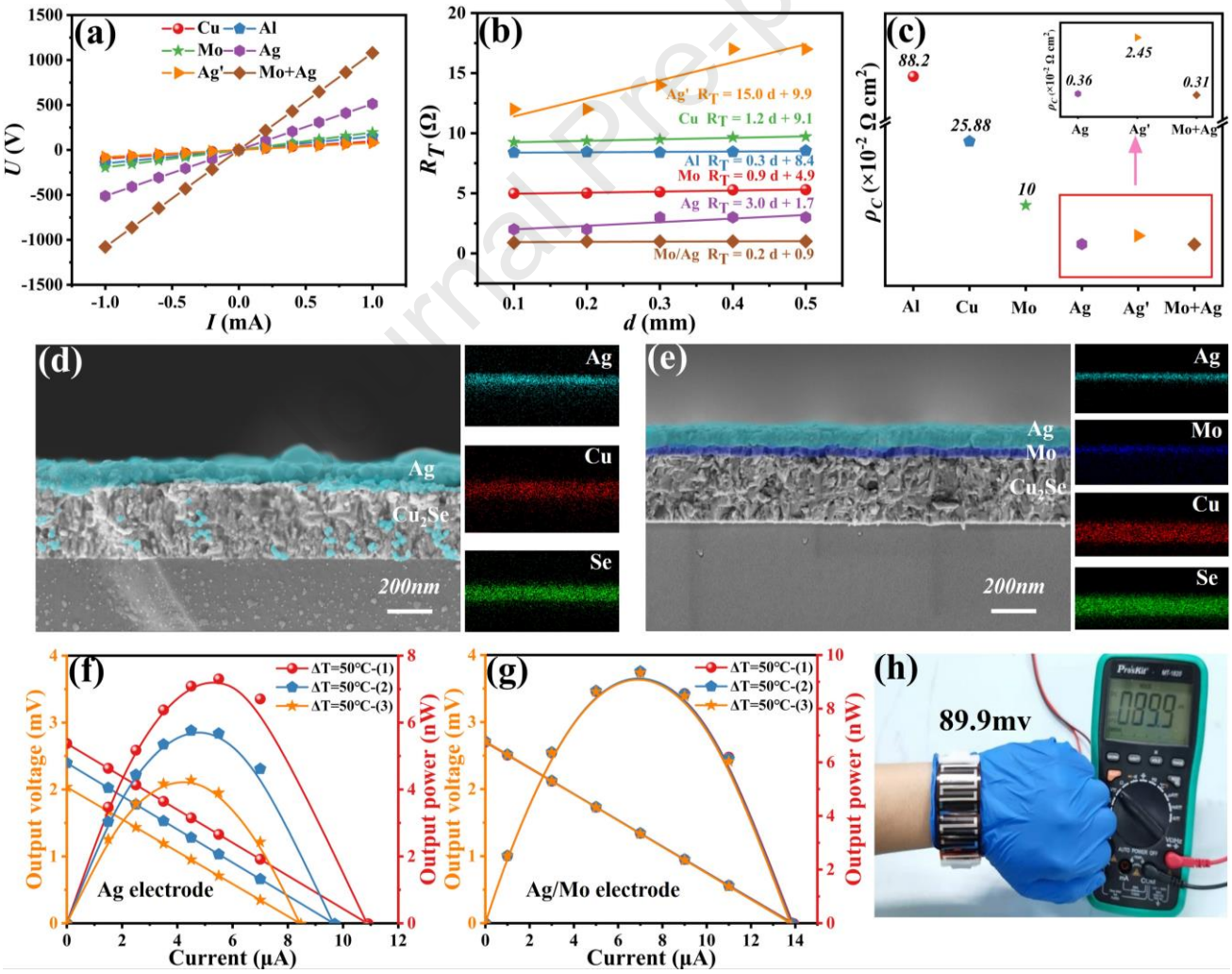

Fig.5. Comparison of (a) IV curves, (b) total resistance R_T and (c) contact resistivity ρ_c when using

different metal electrodes. Cross section morphology and element mappings of films with (d) Ag electrode and (e) Ag/Mo composited electrodes after heat treatment. Repeatability test results of I-V and I-P curves for the device at same temperature difference of 50℃ by using (f) single Ag electrode and (g) Ag/Mo composited electrode (Only one tenth of the final number of devices is used for electrode test data). (h) Image of as fabricated flexible device wrapped around the wrist and test the output signal when apply a temperature difference between two ends.

Based on the good thermoelectric properties as demonstrated above, we further investigate the practical applicability of the Cu_2Se based flexible thin films. It is well-known that the total resistance of the device should be as low as possible to ensure high performance of the device. Therefore, selecting a suitable and accurate metal electrode is one of the key procedures to assembly device as the resistance of composed material itself is almost unchanged during the operation. We, firstly, deposited different kinds of metal electrodes on as-fabricated Cu_2Se films and measure U-I characteristic curve to check the contact resistance between the film and metal electrodes (Fig. 5a). The contact between metal and Cu_2Se film is divided into Schottky contact and low resistance ohmic contact, the actual situation of which kind of contact depends on the material characteristics between metal and semi-conductor [36-38]. Four common single metal electrodes, including Cu, Al, Mo and Ag are performed in this work. Fig.5 (a) to Fig.5 (c) show the basis tests for electrode selection, based on TLM (Transmission Line Model) measurement principle [39], which model construction and physical demonstration is provided in Fig.S9 (Supporting Information). TLM is a measurement method that uses metal electrodes of the same length and width to be uniformly arranged on the thin film. The total resistance between adjacent metal electrodes can be measured by the difference of electrode spacing. The IV curves of each metal electrode (Fig. 5(a)) show the highest voltage when

employing Ag electrode under the same current. This phenomenon also precisely corresponds to the lowest total resistance (R_T) obtained by different metal electrodes at different distances, as shown in Fig.5 (b). It is worth mentioning that the theoretical value of resistance between two adjacent electrodes can be calculated by the formula [40]:$R_T = 2R_m + 2R_c + R_{semi}$, where R_m is the resistance of the metal electrode, which is usually very small and can be ignored; R_C is the contact resistance between the metal and the semiconductor, R_{semi} is the resistance of the semiconductor. The actual situation is that R_C often changes with temperature, that is, the temperature difference will bring about the difference between theory and practice. In order to facilitate calculation, R_C is a fixed value by default. Therefore, the difference between theoretical resistance and experimental resistance will not be large and within a controllable range. We also check the contact resistivity (ρ_c) to characterize the ohmic contact quality, the ρ_c is generally expressed as following formula: $\rho_c = R_C L_T W$ where L_T is the spacing between electrodes and W is the width of single electrode. The lower the contact resistivity means the better ohmic contact quality. It can be found that Ag electrode exhibit lower ρ_c (0.36×10^{-2} $\Omega\bullet cm^2$) than other metal electrodes. However, Ag electrode is not adopted as the final choice as the Ag diffuses into Cu_2Se layer (Fig. 5d) after heat treatment above 275℃ (the cross-sections of Ag electrode bonded with Cu_2Se before heating can be found in Fig.S10a,Supporting Information), which deteriorates the chemical stability of as fabricated film. The deterioration in ohmic contact can be further confirmed from the result of U-I curve, R_T and ρ_c in Fig. 5a-5c. Hence, we set a Mo layer with a thickness of ~ 50 nm, which possesses better chemical stability, between Ag electrode and Cu_2Se based film (See the SEM image in Fig.5(e)), expecting to block the diffusion of Ag. Qiu *et al.* also used the Mo as diffusion barriers on the $Cu_2Se/Yb_{0.3}Co_4Sb_{12}$ TE couples used in the module to block the the diffusion of Cu [41]. The experimental results also proves that this approach is effective. The

films bonded with composited Ag/Mo electrode shows a much higher voltage than the other metal electrodes at the same current (Fig.5 (a)), as well as a lower total resistance (Fig.5 (b)) and better contact quality (Fig.5 (c)). More importantly, the Ag diffusion is effectively restrained after heat treatment by using the composited electrode, which is clearly shown in Fig. 5 (e). The cross-section mapping images of Ag/Mo composited electrode bonded Cu_2Se film before heating can be found in Fig.S10b (Supporting Information). A flexible thermoelectric device consisting of 10 Cu_2Se films (26 mmx2 mmx450 nm) is fabricated on PI substrates connected with silver paste (Fig. S11,Supporting Information). It can be seen that the current-voltage (I-V) and current-power (I-P) curves for the device at different temperature difference ($\Delta T = T_{hot} - T_{cold}$) from 20 to 50℃ in Fig. S12 (a) (Supporting Information). The highest output power ~ 70 nW and calculated maximum power density of 4.28 Wm^{-2} are obtained when the output current is 5.8 μA under the temperature difference of 50℃. In Fig.5 (f) and Fig.5 (g), we plot the repeatability test results of I-V and I-P curves for the device at same temperature difference of 50℃ by using single Ag electrode, and Ag/Mo composited electrode, respectively. It can be found that the output power decreased during the repeatability test when using single Ag electrode, which corresponds with the deterioration of ohmic contact originated from the Ag diffusion in the Cu_2Se film (Fig. 5 (d)). While the output powers of the device demonstrate no attenuation when using the Ag/Mo composited electrode, further confirming enhancement of the stability for the device. Based on the good flexibility of as-fabricated device (Fig. S12 (b), Supporting Information), we can wrap the device around the wrist with wire and a schematic diagram of a specific thermoelectric device as shown in Fig.5 (h) and Fig.S11 (Supporting Information). When there is a certain temperature difference between the upper and lower ends of the device, the multi-meter displays the corresponding voltage. Here, the relatively temperature difference is built by heating one

end of the device advanced. The picture shown proves the superiority of flexible device, indicating its big potential in applying on the wearable devices.

4. Conclusions

In this work, highly (0*l*0) orientation flexible Cu_2Se films with variable Cu/Se ratios were fabricated by a facile co-sputtering method. Excess Cu in the Cu_2Se films played important roles in optimizing the carrier concentration by suppressing the formation of Cu vacancies and donating electrons, leading to the high Seebeck coefficient. The highly (0*l*0) preferred orientation contributed to high carrier mobility and maintained decent electrical conductivity. As a result, an excellent *PF* of 11.12 $\mu Wcm^{-1}K^{-2}$ was obtained for Cu_2Se based film at 275℃. Combined with the low thermal conductivity of as-fabricated films, a maximum *ZT* of 0.42 was achieved at 275℃. Subsequently, the thermal stability of the flexible thermoelectric device assembled with high performance Cu_2Se films was greatly improved after introducing a Mo buffer layer into electrode layer. The maximum power density of 4.28 Wm^{-2} was achieved at a temperature difference of 50 ℃, demonstrating its potential in wearable applications.

Acknowledgements

This work is supported by National Natural Science Foundation of China (No.11604212), Guangdong Basic and Applied Basic Research Foundation (2019A1515110107 and 2020A1515010515), and Science and Technology plan project of Shenzhen (20200811230408001). The authors are thankful for the assistance on HAADF-STEM observation received from the Electron Microscope Center of the Shenzhen University.

References

[1] X.L. Shi, J. Zou, Z. G. Chen, Chem. Rev. 120 (2020) 7399.

[2] Y.X. Chen, X.L. Shi, Z.H. Zheng, F. Li, W.D. Liu, W.Y. Chen, X.R. Li, G.X. Liang, J.T. Luo, P.

Fan, Mater. Today Phys. 16 (2021):100306.

[3] J. Tang, C. Qin, H.L. Yu, Z.Z. Zeng, L.X. Cheng, B.H. Ge, Y. Chen, W. Li, Y.Z. Pei, Mater. Today Phys. 22 (2022):100591.

[4] C. Tan, X. Tan, F. Shi, Y. Yin, G.Q. Liu, C. Xiong, H. Wang, G. Luo, B. Yu, J.G. Noudem, B. Liang, J. Jiang, Ceram. Int. 47 (2021) 725.

[5] C. Li, S. Ma, P. Wei, W. Zhu, X. Nie, X. Sang, Z. Sun, Q. Zhang, W. Zhao, Energ. Environ. Sci. 13 (2020) 535.

[6] O.E. Femi, N. Ravishankar, K. Chattopadhyay, J. Mater. Sci. 51 (2016) 7254.

[7] X. Guo, J. Qin, X. Jia, D. Jiang, Inorg. Chem. Front. 5 (2018) 1540.

[8] L.D. Zhao, S.H. Lo, Y. Zhang, H. Sun, G. Tan, C. Uher, C. Wolverton, V.P. Dravid, M.G. Kanatzidis, Nature 508 (2014) 373.

[9] L.D. Zhao, H.J. Wu, S.Q. Hao, C.I. Wu, X.Y. Zhou, K. Biswas, J.Q. He, T.P. Hogan, C. Uher, C. Wolverton, V.P. Dravid, M.G. Kanatzidis, Energ. Environ. Sci. 6 (2013) 3346.

[10] W. Wei, C. Chang, T. Yang, J. Liu, H. Tang, J. Zhang, Y. Li, F. Xu, Z. Zhang, J.F. Li, G. Tang, J. Am. Chem. Soc. 140 (2018) 499.

[11] J. Dong, F.H. Sun, H. Tang, J. Pei, H.L. Zhuang, H.H. Hu, B.P. Zhang, Y. Pan, J.F. Li, Energ. Environ. Sci. 12 (2019) 1396.

[12] L. Yang, Z.G. Chen, G. Han, M. Hong, Y. Zou, J. Zou, Nano Energy 16 (2015) 367.

[13] Z.X. Zhang, K.P. Zhao, T.R. Wei, P.F. Qiu, L.D.Chen, X. Shi, Energy Environ. Sci. 13 (2020) 3307.

[14] B. Zhong, Y. Zhang, W. Li, Z. Chen, J. Cui, W. Li, Y. Xie, Q. Hao, Q. He, Appl. Phys. Lett. 105 (2014):123902.

[15] A.A. Olvera, N.A. Moroz, P. Sahoo, P. Ren, T.P. Bailey, A.A. Page, C. Uher, P.F.P. Poudeu, Energ. Environ. Sci. 10 (2017) 1668.

[16] Y.Y. Li, X.Y. Qin, D. Li, J. Zhang, C. Li, Y.F. Liu, C.J. Song, H.X. Xin, H.F. Guo, Appl. Phys. Lett. 108 (2016):062104.

[17] L.L. Yang, J.T. Wei, Y. Qin, L. Wei, P. Song, M. Zhang, F. Yang, X. Wang, Mater. (Basel) 14 (2021) 2075.

[18] Z.P. Wu, J.L. Wu, Y. Li, G. Li, Ceram. Int. 46 (2020) 21617.

[19] Y.H. Lv, J. Chen, R.K. Zheng, X. Shi, J. Song, T. Zhang, X. Li, L. Chen, Ceram. Int. 41 (2015) 7439.

[20] M.R. Scimeca, F. Yang, E. Zaia, N. Chen, P. Zhao, M.P. Gordon, J.D. Forster, Y.-S. Liu, J. Guo, J.J. Urban, A. Sahu, ACS. Appl. Energ. Mater. 2 (2019) 1517.

[21] L.D. Chen, S.H.I Xun, Y.L. Li, M. Dobeli, J.K. Chen, Y.H. LV, J. Inorg. Mater. 30 (2015) 1115.

[22] Y. Jin, J. Hwang, S. Kim, J. Kim, S.J. Kim, Nano. Adv. 3 (2021) 3107.

[23] J. Chen, D. Bao, Q. Sun, W.D. Liu, C. Liu, J. Tang, L. Yang, D. Zhou, M.S. Dargusch, Z.G. Chen, J. Solid State Chem. 296 (2021):121987.

[24] X.L. Huang, D.W. Ao, T.B. Chen, Y.X. Chen, F. Li, S. Chen, G.X. Liang, X.H. Zhang, Z.H. Zheng, P. Fan, Mater. Today Energ. 21 (2021):100743.

[25] P. Fan, X.L. Huang, T.B. Chen, F. Li, Y.X. Chen, B. Jabar, S. Chen, H.L. Ma, G.X. Liang, J.T. Luo, X.H. Zhang, Z.H. Zheng, Chem. Eng. J. 410 (2021):128444.

[26] V. Linseis, F. Volklein, H. Reith, K. Nielsch, P. Woias, Rev. Sci. Instrum. 89 (2018) 015110.

[27] W. Shi, J. Lian, Int. J. Hydrogen. Energ. 44 (2019) 22983.

[28] L. Zhu, Y. He, D. Zhou, Expert. Syst. Appl. 116 (2019) 430.

[29] Z.M. Yue, K.P. Zhao, H.Y. Chen, P.F. Qiu, L.D. Chen, X. Shi, Chin. Phys. Lett. 38 (2021) 117201.

[30] D. Yang, X. Su, J. Li, H. Bai, S. Wang, Z. Li, H. Tang, K. Tang, T. Luo, Y. Yan, J. Wu, J. Yang, Q. Zhang, C. Uher, M.G. Kanatzidis, X. Tang, Adv. Mater. 32 (2020) e2003730.

[31] W.D. Liu, L. Yang, Z.G. Chen, Nano Today 35 (2020):100938.

[32] Y. Lu, Y. Ding, Y. Qiu, K. Cai, Q. Yao, H. Song, L. Tong, J. He, L. Chen, ACS. Appl. Mater. Inter. 11 (2019) 12819.

[33] Y.D. Li, P. Fan, Z.H. Zheng, J.T. Luo, G.X. Liang, S.Z. Guo, J. Alloy. Compd. 658 (2016) 880.

[34] Z.Y. Lin, C. Hollar, J.S. Kang, A. Yin, Y. Wang, H.Y. Shiu, Y. Huang, Y. Hu, Y. Zhang, X. Duan, Adv. Mater. 29 (2017):1606662.

[35] J.L. Yu, K.P. Zhao, P.F. Qiu, X. Shi, L.D. Chen, Ceram. Int. 43 (2017) 11142.

[36] M. Yin, A. Zhong, J. Luo, F. Li, Z. Zheng, P. Fan, J. Electron. Mater. 46 (2016) 3256.

[37] T. Jang, J.S. Kwak, O.H. Nam, Y. Park, Solid State Electron. 50 (2006) 433.

[38] D.M. Mitin, F.Y. Soldatenkov, A.M. Mozharov, A.A. Vasil'ev, V.V. Neplokh, I.S. Mukhin, Nanosyst. Phys. Chem. Math. 9 (2018) 789.

[39] M.A. Khan, J.N. Kuznia, J.M. Van Hove, N. Pan, J. Carter, Appl. Phys. Lett. 60 (1992) 3027.

[40] Z.H. Sun, H.L. Huang, Y.H. Liu, Y.A. Yin, K.R. Qin, P.C. Tao, K. Liu, N. Sun, IEEE. T. Electron. Dev. 68 (2021) 299.

[41] P.F. Qiu, T. Mao, Z.F. Huang, X.G. Xia, J.C. Liao, M.T. Agne, M. Gu, Q.H. Zhang, D.D. Ren, S.Q. Bai, X. Shi, J. Snyder, L.D. Chen, Joule 3 (2019) 1538.

Highlights

(1) Flexible Cu_2Se based thin films with desired highly (0*l*0)-preferred orientation were successfully achieved by optimized growth temperature and composition;

(2) Introduced excess Cu in flexible Cu_2Se films contribute to the improvement electrical and thermal transport properties simultaneously;

(3) A Mo buffer layer is innovatively introduced into electrode layer, greatly enhance the thermal stability of flexible thermoelectric device assembled with high performance Cu_2Se films.

Declaration of interests

☒ The authors declare that they have no known competing financial interests or personal relationships that could have appeared to influence the work reported in this paper.

☐ The authors declare the following financial interests/personal relationships which may be considered as potential competing interests: